

# Catalytic Response and Stability of Nickel/Alumina for the Hydrogenation of 5-Hydroxymethylfurfural in Water

Noémie Perret, Alexios Grigoropoulos, Marco Zanella, Troy D. Manning, John B. Claridge, and Matthew J. Rosseinsky\*<sup>[a]</sup>

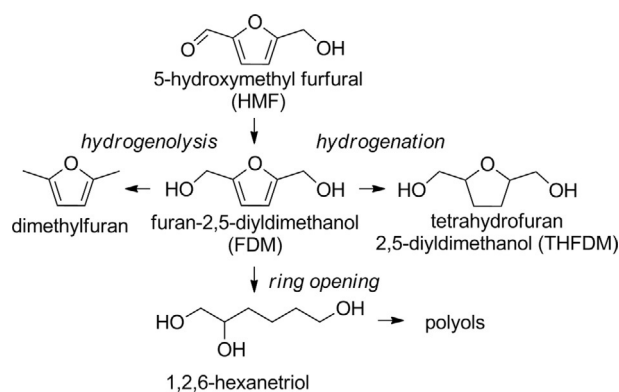
The catalytic response of Ni on Al<sub>2</sub>O<sub>3</sub> obtained from Ni–Al layered double hydroxides was studied for the liquid-phase hydrogenation of hydroxymethyl furfural to tetrahydrofuran-2,5-diylldimethanol (THFDM) in water. The successive calcination and reduction of the precursors caused the removal of interlayer hydroxyl and carbonate groups and the reduction of Ni<sup>2+</sup> to Ni<sup>0</sup>. Four reduced mixed oxide catalysts were obtained, consisting of different amount of Ni metal contents (47–68 wt%) on an Al-rich amorphous component. The catalytic activity was

linked to Ni content whereas selectivity was mainly affected by reaction temperature. THFDM was formed in a stepwise manner at low temperature (353 K) whereas 3-hydroxymethyl cyclopentanone was generated at higher temperature. Coke formation caused deactivation; however, the catalytic activity can be regenerated using heat treatment. The results establish Ni on Al<sub>2</sub>O<sub>3</sub> as a promising catalyst for the production of THFDM in water.

## Introduction

As the production of biofuels and bioenergy from biomass remains economically challenging, there is a growing demand for the co-production of value-added chemicals to render the process cost effective. Cellulose and hemicelluloses, the two major components of lignocellulosic biomass, can be broken down and converted to monosaccharides.<sup>[1]</sup> The subsequent dehydration of six-carbon sugars can generate 5-hydroxymethylfurfural (HMF), which is regarded as a primary renewable building block.<sup>[2–5]</sup> The hydrogenolysis of biomass and the subsequent dehydration are mainly carried out in water, but the extraction of furanic products remains challenging.<sup>[3,6,7]</sup> Therefore the use of water as solvent for the subsequent transformation of HMF is of great importance, and these reactions require heterogeneous catalysts that exhibit high activity, selectivity and stability in aqueous solutions.

The conversion of HMF into value-added chemicals has received increasing interest over the last decade<sup>[2,3,8,9]</sup> during which a wide variety of heterogeneous metal (i.e., Ni, Cu, Pd, Pt, Ru)-supported catalysts were studied.<sup>[10,11]</sup> Although most research focused on C–O hydrogenolysis (e.g., dimethyl furan) and ring-opening products (e.g., hexanetriol, C<sub>5</sub> and C<sub>6</sub> polyols), there are fewer reports on the selective hydrogenation of HMF towards tetrahydrofuran-2,5-diylldimethanol (THFDM; Scheme 1). This chemical finds application as a solvent (e.g.,



**Scheme 1.** Reaction pathway for the transformation of HMF to some of the targeted compounds in the literature.

for the dehydration of fructose), a building block for the synthesis of polymers (e.g., synthesis of polyesters via caprolactone)<sup>[12]</sup> and high-value chemicals (e.g., 8-oxa-3-aza-bicyclo(3.2.1)octane hydrochloride).<sup>[13]</sup>

A number of factors have been proposed to influence the catalytic response, including the nature of the catalysts and reaction conditions, that is, the solvent,<sup>[14]</sup> pH value (acidic or neutral),<sup>[15]</sup> hydrogen partial pressure,<sup>[16]</sup> temperature,<sup>[16]</sup> metal, isoelectric point (IEP), acid and basic properties of the support.<sup>[7,15]</sup> Indeed, the nature of the metal affects the selectivity for which Cu- and Ru-based catalysts can be selective for C–O hydrogenolysis with formation of dimethyl furan<sup>[17,18]</sup> whereas polymerisation of the intermediate (furan-2,5-diylldimethanol (FDM); Scheme 1) occurs over Pd and Pt catalysts.<sup>[15]</sup>

On the other hand, incorporation of Ni on Pd/SiO<sub>2</sub> and Co–Al mixed-oxide catalysts results in concomitant hydrogenation of the ring and formation of the saturated THFDM derivative, with a 96% yield over Ni–Pd/SiO<sub>2</sub><sup>[11]</sup> and 89% over Ni–Co–Al

[a] N. Perret, A. Grigoropoulos, M. Zanella, T. D. Manning, J. B. Claridge, Prof. M. J. Rosseinsky  
Department of Chemistry  
University of Liverpool  
Crown Street, Liverpool, L69 7ZD (UK)  
E-mail: m.j.rosseinsky@liv.ac.uk

Supporting Information for this article is available on the WWW under <http://dx.doi.org/10.1002/cssc.201501225>. Underlying data can be accessed at <http://dx.doi.org/10.17638/datacat.liverpool.ac.uk/61>.

mixed oxides.<sup>[16]</sup> It is worth noting that Raney Ni<sup>[12,13,19]</sup> exhibits 100% selectivity towards THFDM, but it is less active than other supported Ni catalysts (e.g., Ni–Pd/SiO<sub>2</sub>) for this reaction.<sup>[11,16]</sup> It was also shown that supports with a high IEP (e.g., Al<sub>2</sub>O<sub>3</sub>) favour hydrogenation of the ring whereas supports exhibiting Brønsted acidity, such as SiO<sub>2</sub>, generate polyols and polymers via ring opening.<sup>[15,20]</sup> Despite these reports,<sup>[11,13,15,16,20]</sup> which suggest that Ni metal and Al<sub>2</sub>O<sub>3</sub> favour the formation of THFDM, the hydrogenation of HMF over Ni on Al<sub>2</sub>O<sub>3</sub> has not been studied in a systematic manner.

The environment can cause degradation of heterogeneous catalysts, and stability in water remains challenging as changes in physical structure easily occur.<sup>[21]</sup> The studies over Raney Ni were conducted in organic solvents such as alcohols (e.g., ethanol)<sup>[19]</sup> and ethyl acetate.<sup>[13]</sup> Nakagawa and Tomishige<sup>[11]</sup> tested Ni–Pd/SiO<sub>2</sub> as a catalyst for the same reaction in water and they observed that 16% of Ni leached into the liquid phase after 2 h.

Raney Ni can exhibit 100% selectivity towards THFDM. However, its preparation requires dissolving Ni in molten Al, quenching and treatment of the alloy with NaOH (ca. 5 M) to leach Al out. As a result, a large amount of concentrated NaOH is used during synthesis, the material is pyrophoric and its chemical composition cannot be easily controlled. Therefore, catalysts that are easier to synthesise and handle are required, if the hydrogenation of HMF is to be carried out in a more environmentally benign process using water as the solvent. The use of water as a solvent in sustainable chemical processes is preferred as it is non-toxic, non-flammable, low cost, renewable and widely available.<sup>[22,23]</sup>

There has been a growing interest, in recent years, in the synthesis of mixed oxides by thermal pre-treatment of layered double hydroxides (LDH) and their use for hydrogenation reactions.<sup>[24]</sup> The mixed oxides obtained can exhibit distinct properties compared to traditional impregnated metal catalysts including small crystallite size, large surface area, good stability, high metal loading, basic properties and distinct catalytic performance.<sup>[25–27]</sup> After reduction, the catalysts display well-dispersed metallic particles on the surface and enhanced metal–oxide interaction.<sup>[24]</sup> Hence, the supported Ni catalysts used in this study were derived from Ni–Al layered double hydroxides.

In this work, the catalytic response of Ni on Al<sub>2</sub>O<sub>3</sub> catalysts for the hydrogenation of HMF in water is presented. The catalysts are prepared from layered double hydroxides of readily available non-noble metals under mild conditions in water. The

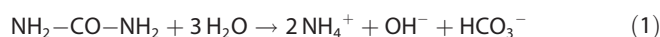
effect of catalyst composition and reaction conditions is also systematically investigated; the chemical kinetics of this reaction and the catalytic stability of the catalysts are also considered.

## Results and Discussion

### Characterisation measurements

#### Layered double hydroxides precursors

Layered double hydroxides are composed of hydroxide brucite-like sheets where two metals (M<sup>2+</sup>, M<sup>3+</sup>) occupy octahedral sites; the presence of M<sup>3+</sup> cations generates a net positive charge, which is balanced by interlayers composed of anions and water.<sup>[28]</sup> In this work, M<sup>3+</sup> = Al<sup>3+</sup>, M<sup>2+</sup> = Ni<sup>2+</sup> have been introduced as cations whereas CO<sub>3</sub><sup>2–</sup> is the charge-balancing anion; the general formula can be written as [Ni<sup>II</sup><sub>1–x</sub>Al<sup>III</sup><sub>x</sub>(OH)<sub>2</sub>][CO<sub>3</sub><sup>2–</sup>]<sub>x/2</sub>·mH<sub>2</sub>O. The precursors were synthesised by precipitation from an aqueous solution of NiCl<sub>2</sub>·6H<sub>2</sub>O and AlCl<sub>3</sub>·6H<sub>2</sub>O using urea, based on the method of Costantino et al.<sup>[29]</sup> The change in temperature (from 295 to 368 K at 1 Kmin<sup>–1</sup>) results in the decomposition of urea according to Reaction (1).<sup>[30]</sup>



The pH value progressively increased to circa 8.5, which is suitable to precipitate the metal hydroxides. The urea hydrolysis takes place slowly and uniformly, so the precipitation is carried out under a low degree of supersaturation.<sup>[31]</sup> The predominant species in the carbonate equilibria at final pH (≈8.5) is hydrogen carbonate,<sup>[32]</sup> providing the required interlayer anion. Four layered double hydroxides (NiAl-P) were prepared with different Ni–Al ratios (x = 0.24, 0.28, 0.36, 0.47); the increasing Z number (NiAl-ZP) relates to the increasing Al content (Table 1). The crystalline structure and textural properties were investigated by inductively coupled plasma–optical emission spectroscopy (ICP–OES), X-ray diffraction (XRD), CHN analysis, thermogravimetric analysis (TGA), scanning electron microscopy–energy-dispersive X-ray spectroscopy (SEM–EDX), Fourier transform infrared (FTIR) and nitrogen physisorption experiments.

The XRD pattern of the Ni–Al precursors (taking the sample with the lowest Al content, NiAl-1P, as representative, Figure 1 a) shows seven peaks (2θ = 13–78°) that are characteristic of Ni–Al layered double hydroxides.<sup>[33]</sup> The degree of crystallini-

**Table 1.** Composition, surface area and crystal parameters associated with the precursors.

Catalyst	Composition <sup>[a]</sup>	x <sup>[b]</sup>	SA <sup>[c]</sup> [m <sup>2</sup> g <sup>–1</sup> ]	a <sup>[d]</sup> [Å]	c <sup>[d]</sup> [Å]	d <sub>LDH</sub> <sup>[e]</sup> [nm]
NiAl-1P	Ni <sub>0.76</sub> Al <sub>0.24</sub> (OH) <sub>2</sub> (CO <sub>3</sub> ) <sub>0.12</sub> ·0.64 H <sub>2</sub> O	0.24/0.26	65	3.061(1)	23.46(1)	10(1)
NiAl-2P	Ni <sub>0.72</sub> Al <sub>0.28</sub> (OH) <sub>2</sub> (CO <sub>3</sub> ) <sub>0.14</sub> ·0.58 H <sub>2</sub> O	0.28/0.28	67	3.057(1)	23.52(1)	10(1)
NiAl-3P	Ni <sub>0.64</sub> Al <sub>0.36</sub> (OH) <sub>2</sub> (CO <sub>3</sub> ) <sub>0.18</sub> ·0.45 H <sub>2</sub> O	0.36/0.34	84	3.048(1)	23.37(1)	10(1)
NiAl-4P	Ni <sub>0.53</sub> Al <sub>0.47</sub> (OH) <sub>2</sub> (CO <sub>3</sub> ) <sub>0.23</sub> ·0.30 H <sub>2</sub> O	0.47/0.51	107	3.037(1)	23.06(1)	10(1)

[a] based on ICP, CHN and TGA analysis. [b] Al ratio determined from ICP analysis after digestion in HCl/from SEM–EDX measurements. [c] BET surface area calculated from N<sub>2</sub> adsorption–desorption isotherms. [d] Lattice parameters based on R3̄m space group, errors equate to 3σ. [e] Crystallite size based on Double-Voigt approach, errors equate to 1σ.

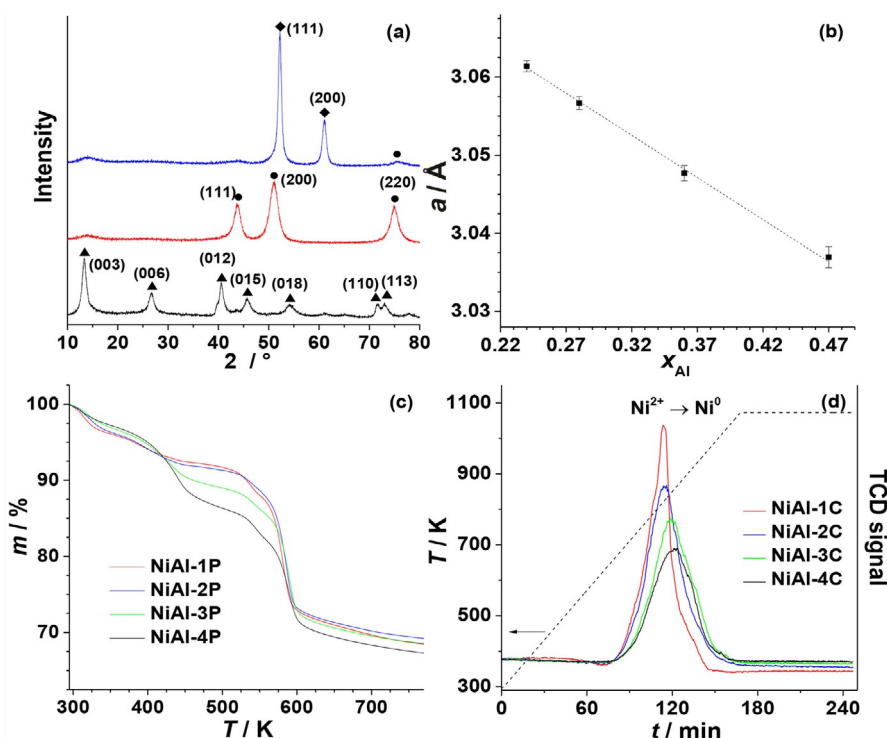


**Figure 1.** (a) XRD patterns of NiAl-1 precursor (black), calcined (red) and reduced (blue) showing also the main planes associated with Ni (◆), NiO (●) and hydroxalcite (▲); (b) lattice parameter  $a$  of the precursors as a function of Al bulk molar ratio ( $x$ ) where the linear fit obeys Vegard's law; (c) TGA profiles for the precursors (P) and (d)  $H_2$ -TPR profiles (with temperature ramp in dotted line) generated for the calcined (C) samples of NiAl-1, NiAl-2, NiAl-3 and NiAl-4.

ty and textural properties depend on various reaction parameters such as pH value, temperature, concentration and aging of the precipitate.<sup>[26,34]</sup> The samples present good crystallinity in agreement with the work of Costantino et al.,<sup>[29]</sup> who reported improved crystallinity with longer digestion time (> 36 h) at temperatures of 363–373 K.

The FTIR spectra (taking NiAl-1P as representative, Figure S1 in the Supporting Information) show a broad band at  $3530\text{ cm}^{-1}$ , which is mainly attributed to Al-coordinated OH groups with small contributions of H-bonded interlayer water,  $\text{CO}_3^{2-}$ -H<sub>2</sub>O bridging and hydroxyl coordinated by both Ni and Al.<sup>[35]</sup> The region between  $1200$ – $1800\text{ cm}^{-1}$  is characterised by the bending mode of interlayer water around  $1655\text{ cm}^{-1}$  ( $1640$ – $1700\text{ cm}^{-1}$ )<sup>[35]</sup> and interlayer carbonate at  $1366\text{ cm}^{-1}$  ( $1350$ – $1400\text{ cm}^{-1}$ ).<sup>[35]</sup> These results confirm the presence of H<sub>2</sub>O and  $\text{CO}_3^{2-}$  in the interlayer and are in agreement with hydroxide sheets.

The analysis by ICP of Al and Ni contents of the supernatant (<0.1% metal in solution) and the precursors after digestion ( $x_{\text{Al}}$ , Table 1) verified that complete precipitation of the metal hydroxides occurred. The CHN results were in agreement ( $\pm 5\%$ ) with the theoretical amount of  $\text{CO}_3^{2-}$  and H<sub>2</sub>O in the interlayer (according to the Miyata formula),<sup>[36]</sup> the compositions of the four layered double hydroxides are presented in Table 1.

XRD patterns over a larger  $2\theta$  range ( $10^\circ$ – $120^\circ$ ) and with an internal standard were measured to determine the lattice parameters ( $a$ ,  $c$ ; Table 1); they were obtained by fitting the patterns using a  $R\bar{3}m$  rhombohedral symmetry unit cell.  $c$  corresponds to three times the thickness of a unit layer; hence, it is

related to the interlayer and depends on factors such as the nature and concentration of the anion, the state of hydration, the strength of hydrogen bond between the anions and the hydroxyl groups.<sup>[28]</sup>  $a$  is associated with the cation–cation distance in the hydroxide layer; as the radius of  $\text{Al}^{3+}$  ( $0.50\text{ \AA}$ ) is smaller than  $\text{Ni}^{2+}$  ( $0.69\text{ \AA}$ ),  $a$  decreases with increasing Al content. Applicability of Vegard's law can be tested (Figure 1b) using Equation (2),

$$a = a_{\text{Ni}} + x \times (a_{\text{Al}} - a_{\text{Ni}}) \quad (2)$$

where  $x$  and  $a_{\text{Ni}}$  and  $a_{\text{Al}}$  correspond to the molar fraction of Al and the lattice parameters of the pure constituents, respectively. The linear fitting confirms the validity of Vegard's law; moreover, the extrapolation of  $a_{\text{Ni}}$  ( $x=0$ ,  $a_{\text{Ni}}=3.08\text{ \AA}$ ) is close to that of brucite-like  $\text{Ni}(\text{OH})_2$  ( $3.11\text{ \AA}$ ).<sup>[37]</sup>

A representative SEM image using NiAl-4P as example is presented in Figure 2a where the lamellar/platelet morphology observed for the four samples is characteristic of a well-developed layered structure. EDX measurements confirm the homogeneity of the samples, and the Al ratios (Table 1) are close ( $\pm 8\%$ ) to those obtained by ICP. The Brunauer–Emmett–Teller (BET) surface areas ( $\text{SA}=65$ – $107\text{ m}^2\text{ g}^{-1}$ , Table 1) are within the range of values reported in the literature for Ni–Al layer double hydroxides ( $15$ – $98\text{ m}^2\text{ g}^{-1}$ )<sup>[38–40]</sup> and increase with the Al content whereas the crystallite size ( $d_{\text{LDH}}=10\text{ nm}$ ) remains constant.

### Catalyst pre-treatments

The TGA curves of the four systems are shown in Figure 1c. The first mass loss can be attributed to dehydration and partial dehydroxylation whereas the second step is due to the loss of interlayer hydroxyl and carbonate groups.<sup>[41]</sup> NiAl-4P has the lowest amount of water and highest quantity of carbonate in the interlayer (see composition, Table 1); hence, it has the lowest mass loss during the first step and the highest during the second step. The four layered double hydroxides have similar temperatures for the two steps (ca. 373 and 550 K). The loss of the interlayer groups is associated with an increase of the surface area by 50–80%. Based on the TGA results, all samples were calcined at 773 K (denoted as NiAl-C). The XRD patterns of NiAl-C after calcination (taking NiAl-1C as representative, Figure 1a) show three peaks ( $2\theta = 43\text{--}75^\circ$ ) that are characteristic of cubic NiO. There is no detectable signal corresponding to  $\text{Al}_2\text{O}_3$  or spinel (e.g.,  $\text{NiAl}_2\text{O}_4$ ); this is not surprising as higher calcination temperatures ( $> 1100$  K) are usually required for their formation.<sup>[42]</sup> Thus, the samples are composed of a mixture of an Al-rich amorphous component and a NiO-like oxide. The decrease of the NiO lattice parameters ( $a$ , Table 2) with increasing Al content and the lower values compared to pure NiO (4.177 Å) suggest that  $\text{Al}^{3+}$  is incorporated into the lattice, which is in agreement with literature.<sup>[26]</sup> The substitution of a divalent host ( $\text{Ni}^{2+}$ ) by a trivalent cation ( $\text{Al}^{3+}$ ) is compensated by the formation of cation vacancies that balance the charge.<sup>[43]</sup> The introduction of  $\text{Al}^{3+}$  is associated with a slight decrease in NiO mean crystallite size (from 6 to 4 nm). The Al-rich amorphous phase contributes significantly to the

surface area of the calcined samples as it increases (Table 2) with a decreasing Ni content.

The hydrogen temperature-programmed reduction ( $\text{H}_2$ -TPR) of the four calcined samples generated the profiles shown in Figure 1d where positive peaks, corresponding to  $\text{H}_2$  consumption, are evident. The amounts of  $\text{H}_2$  consumed (per gram of material) are included in Table 2 and correspond ( $\pm 4\%$ ) to the amount of  $\text{H}_2$  required for the complete reduction of  $\text{Ni}^{2+}$  to  $\text{Ni}^0$ . The temperatures of the peaks at maximum signals ( $T_{\text{max}}$ ) are also included in Table 2 and range from 819 to 859 K. The introduction of  $\text{Al}^{3+}$  into the NiO lattice enhances the stability of  $\text{Ni}^{2+}$  and hinders its reduction; this is a well-established phenomenon<sup>[26,42]</sup> and explains the shift of  $T_{\text{max}}$  to higher temperature with increasing Al content. Finally, the calcined samples were reduced under  $\text{H}_2$  (at 773 K) and passivated; after these pre-treatments, the samples are denoted as NiAl-R.

### Reduced mixed-oxide catalysts

The composition of the four catalysts (Table 3) was determined by ICP, CHN and TGA analysis. As expected, the Al bulk ratios of the reduced catalysts are similar ( $\pm 5\%$ ) to the ones of the precursors (NiAl-P, Table 1). The XRD patterns of NiAl-R (taking NiAl-1R as representative, Figure 1a) show two peaks ( $2\theta = 52\text{--}61^\circ$ ) that can be attributed to cubic nickel metal (ICDD 04-0850). The samples must consist of Ni particles dispersed on the Al-rich amorphous component as no Al-containing phases were observed in the diffraction patterns.  $\text{Ni}^0$  mean crystallite sizes ( $d_{\text{Ni}^0}$ , Table 3) are in the range of 10–14 nm, with an increase in Ni loading corresponding to an increase in crystallite size.  $\text{Ni}^0$  mean crystallite sizes of the reduced samples NiAl-R are twice the size of NiO crystallites (NiAl-C,  $d_{\text{NiO}}$ , Table 2); however, the presence of  $\text{Al}^{3+}$  in NiO lattices after calcination may broaden the peaks due to strain and a direct comparison between crystallite sizes might not be valid.

The morphology of the catalysts was investigated by performing SEM and TEM imaging. Despite the modifications to the composition during pre-treatment, the reduced catalysts (Figure 2b) present a lamellar/platelet structure similar to that of the precursor layered double hydroxides (Figure 2a); the retention of the morphology after calcination and reduction has been already reported elsewhere.<sup>[28,44,45]</sup> TEM-EDX analysis was conducted on NiAl-4R as representative sample; the results obtained suggest that the samples have a good homogeneity ( $x_{\text{Al}} = 0.43 \pm 0.03$ ) and the value obtained is in agreement with

**Table 2.** Ni content and particle properties after calcination as well as  $\text{H}_2$  consumed and maximum temperature during  $\text{H}_2$ -TPR of the calcined samples.

Catalyst	Ni content <sup>[a]</sup> [wt%]	SA <sup>[b]</sup> [m <sup>2</sup> g <sup>-1</sup> ]	$a$ <sup>[c]</sup> [Å]	$d_{\text{NiO}}$ <sup>[d]</sup> [nm]	$\text{H}_2$ consumed [mmol g <sup>-1</sup> ]	$T_{\text{max}}$ [K]
NiAl-1C	68	117	4.159(1)	6.2(6)	11.5(2)	819
NiAl-2C	61	121	4.155(1)	5.1(4)	10.9(2)	828
NiAl-3C	58	142	4.149(1)	4.3(5)	9.5(2)	850
NiAl-4C	47	162	4.145(1)	3.7(6)	8.1(2)	859

[a] Based on ICP analysis after digestion in HCl. [b] Calculated from  $\text{N}_2$  adsorption–desorption isotherms. [c] Lattice parameter based on  $Fm\bar{3}m$  space group, errors equate to  $3\sigma$ . [d] Based on Double-Voigt approach, errors equate to  $1\sigma$ .

**Table 3.** Composition, particle properties and IEP associated with the reduced catalysts.

Catalyst	Composition <sup>[a]</sup>	Ni content <sup>[a]</sup> [wt%]	SA <sup>[b]</sup> [m <sup>2</sup> g <sup>-1</sup> ]	PV <sup>[b]</sup> [cm <sup>3</sup> g <sup>-1</sup> ]	$d_{\text{pore}}$ <sup>[b]</sup> [nm]	$a$ <sup>[c]</sup> [Å]	$d_{\text{Ni}}$ <sup>[d]</sup> [nm]	IEP
NiAl-1R	$\text{Ni}_{0.76}\text{Al}_{0.24}\text{O}_{0.79}\text{H}_{0.28}$	68	89	0.25	10	3.5227(3)	14(1) <sup>[e]</sup>	10.0(2)
NiAl-2R	$\text{Ni}_{0.73}\text{Al}_{0.27}\text{O}_{0.97}\text{H}_{0.24}$	60	101	0.25	10	3.5226(4)	13(1) <sup>[e]</sup>	10.2(2)
NiAl-3R	$\text{Ni}_{0.64}\text{Al}_{0.36}\text{O}_{0.96}\text{H}_{0.33}$	56	113	0.27	9	3.5241(4)	12(1) <sup>[e]</sup>	10.3(2)
NiAl-4R	$\text{Ni}_{0.53}\text{Al}_{0.47}\text{O}_{1.10}\text{H}_{0.39}$	47	129	0.28	9	3.5217(8)	10(1) <sup>[e]</sup> /9(3) <sup>[f]</sup>	10.1(2)

[a] Based on ICP, CHN and TGA analysis. [b] BET surface area, total pore volume and mean pore diameter calculated from  $\text{N}_2$  adsorption–desorption isotherms. [c] Based on  $Fm\bar{3}m$  space group, errors equal to  $3\sigma$ . [d] Mean Ni crystallite size. [e] Based on Double-Voigt approach, errors equate to  $1\sigma$ . [f] From TEM, error equates to  $1\sigma$ .

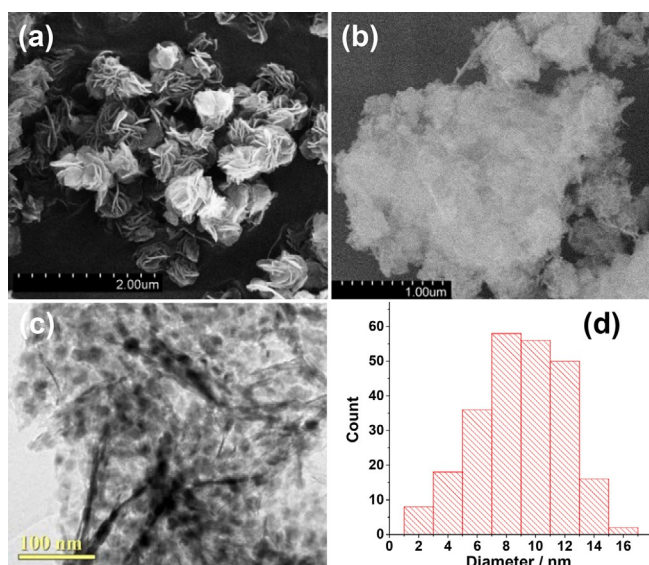


**Figure 2.** Representative (a) SEM and (b, c) TEM images and the corresponding (d) Ni particle size distribution for the precursor NiAl-4P (a) and NiAl-4R after calcination and reduction (b, c, d).

ICP results ( $x_{\text{Al}}=0.47$ ). Chlorine precursors were used for the synthesis of the catalysts, but no chlorine was detected by SEM-EDX analysis (Figure S2). This shows that washing with  $\text{H}_2\text{O}$  followed by treatment with  $\text{NH}_4\text{HCO}_3$  (see the Experimental Section) was enough to remove any residual chlorine. This result is important as chlorine is known to increase metal atom mobility on the support and cause sintering.<sup>[46]</sup> TEM was also employed to determine the Ni particle size distribution and a representative TEM image (for NiAl-4R) is depicted in Figure 2c, showing dispersed pseudo-spherical particles in the 2–16 nm size range (Figure 2d). An essentially equivalent mean size ( $d_{\text{Ni}}$ ) was obtained from the measurements with XRD (10 nm) and TEM (9 nm) analysis (Table 3).

The calcination and reduction of layered double hydroxides (NiAl-P  $\rightarrow$  NiAl-R) was associated with an increase in surface area by 20 to 50%. Moreover, the surface area and total pores volume of the reduced mixed oxide increases with decreasing Ni loading (Table 3). The four catalysts exhibit an average pore size of 9–10 nm. The IEPs were measured; the values obtained are listed in Table 3 and a representative curve of the zeta potential versus pH is shown in Figure S3. The four catalysts have a similar isoelectric point ( $\text{pH}(\text{I}) 10.2 \pm 0.2$ ), which is in agreement with the literature in which values in the pH range 8.5–10.0 were reported for  $\text{Al}_2\text{O}_3$ , boehmite and  $\text{Al}(\text{OH})_3$ .<sup>[47]</sup> We could not find any values reported for Ni metal, but IEPs between pH 7.5 and 10.5 were measured for NiO.<sup>[47]</sup>

To summarise, four catalyst precursors were synthesised by precipitation using urea. XRD, ICP, CHN, SEM-EDX and FTIR measurements confirm full precipitation and formation of layered double hydroxides  $\text{Ni}_{(1-x)}\text{Al}_x(\text{OH})_2(\text{CO}_3)_{x/2} \cdot m\text{H}_2\text{O}$ , with  $0.24 \leq x \leq 0.47$  and  $0.3 \leq m \leq 0.7$ . The successive calcination and reduction of the precursors generated metal on oxide supports. This method of preparation allowed us to synthesise four Ni-on- $\text{Al}_2\text{O}_3$  catalysts with well-dispersed Ni metal particles and high Ni contents (between 47 and 68 wt %).

## Catalytic results

### Kinetic and mechanistic aspects

The hydrogenation of HMF using water as solvent ( $T=353\text{ K}$ ,  $P_{\text{H}_2}=20\text{ bar}$ ) generated a mixture of FDM and THFDM over the four Ni-Al catalysts (NiAl-R, Figure 3a). Control experiments employing  $\gamma\text{-Al}_2\text{O}_3$  or the precursors before (NiAl-P) and after calcination (NiAl-C) did not result in any conversion, suggesting that it is the presence of  $\text{Ni}^0$  particles, formed after reduction of the precursors, which allows for  $\text{H}_2$  uptake on the surface and catalyses the hydrogenation of HMF.

Reaction conditions were chosen to avoid mass transfer limitations. Indeed, the stirring speed and particle size tests were conducted for NiAl-4R (Figure S4) to probe the absence of mass-transfer resistance of the reactants from the gas to the liquid phase (for  $\text{H}_2$ ), from the bulk liquid to the catalyst surface (for HMF and  $\text{H}_2$ ) and internal diffusion resistance.<sup>[48]</sup> The average pore sizes of the four catalysts (9–10 nm, Table 3) are ten times larger than the long axis of HMF (9 Å),<sup>[49]</sup> hence, the pores are sufficiently wide to not impede the passage of the reactants and products of similar size to HMF. Moreover, the stoichiometric ratio of  $\text{H}_2$  to reactant (for converting HMF to THFDM) is above 100. Therefore, applicability of a pseudo-first

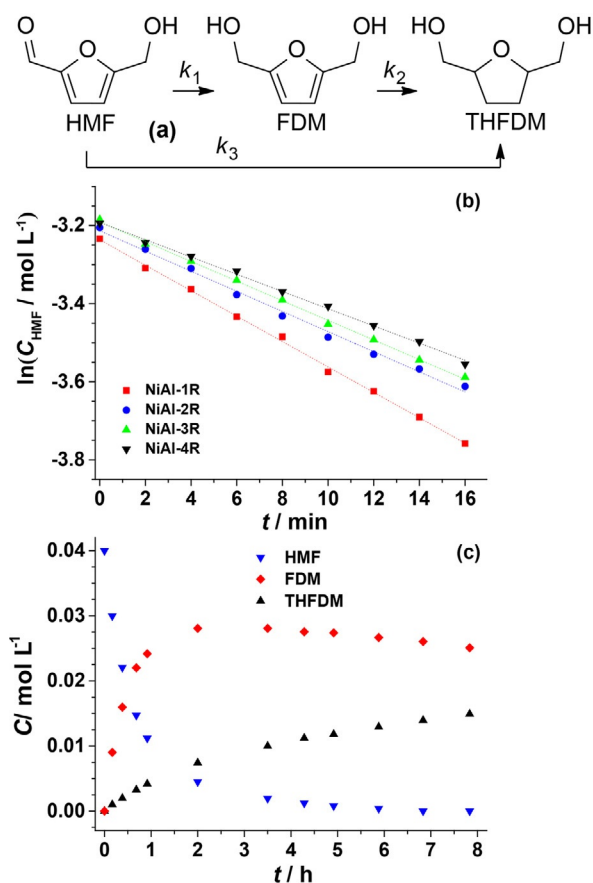


**Figure 3.** (a) Reaction pathway observed for the hydrogenation of HMF at 353 K and  $P_{\text{H}_2}=20\text{ bar}$ . (b) Logarithm of HMF concentration ( $C_{\text{HMF}}$ ) with time ( $t$ ), over 0.03 g catalyst (NiAl-R),  $C_{i,\text{HMF}} \approx 0.04\text{ mol L}^{-1}$ . (c)  $C$  of HMF, FDM and THFDM as a function of time for the hydrogenation of HMF ( $C_{i,\text{HMF}} \approx 0.04\text{ mol L}^{-1}$ ) over 0.04 g NiAl-4R.

order treatment can be tested using the relationship shown in Equation (3):

$$\ln(C_{\text{HMF}}) = \ln(C_{\text{HMF},0}) - kt, \quad (3)$$

where  $C_{\text{HMF}}$  and  $C_{\text{HMF},0}$  represent the concentrations of HMF at time  $t$  and  $t=0$ . The linear relationship between  $\ln(C_{\text{HMF}})$  and  $t$  (Figure 3b) for the four catalysts confirms the adherence to pseudo-first order behaviour. Assuming that deactivation is negligible in these conditions ( $t < 18$  min and conversion under 32%), the initial rate constants ( $k$ ,  $\text{min}^{-1}$ ), listed in Table 4, represent a measure of the intrinsic catalyst activity. We did not observe any induction period associated with cata-

Table 4. Rate constant ( $k$ ) and specific rate constant per mass of Ni ( $k'$ ) and per Ni surface area ( $k''$ ) for the hydrogenation of HMF. <sup>[a]</sup>			
Catalysts	$k$ [ $\text{min}^{-1}$ ]	$k'$ [ $\text{g}_{\text{Ni}}^{-1} \text{min}^{-1}$ ]	$k''$ [ $\text{m}_{\text{Ni}}^{-2} \text{min}^{-1}$ ]
NiAl-1R	0.032	1.5	32
NiAl-2R	0.026	1.4	28
NiAl-3R	0.025	1.5	27
NiAl-4R	0.022	1.5	22

[a] Conditions: 353 K and  $P_{\text{H}_2} = 20$  bar.

lyst activation; therefore, the passivation layer formed during the passivation process (and its removal) does not significantly affect the catalytic response. As shown in Table 4, the  $k$  increases with Ni loading (Table 3), and the four catalysts exhibit equivalent ( $\pm 6\%$ ) specific rate ( $k'$ ) per mass of Ni. The rate constants were converted to specific values ( $k''$ ) using Ni surface areas ( $SA_{\text{Ni}}$ , see the Experimental Section) and are included in Table 4. Although previous studies did not find a clear relation between the activity and the metal particle size (e.g., for Pd-based catalysts<sup>[50]</sup>), our results suggest an increase in  $k''$  with increasing  $d_{\text{Ni}}$ . To the best of our knowledge, this is the first example in which kinetic rates are presented for the hydrogenation of HMF over supported metal catalysts.

Typical temporal dependence of the reactant and molar yields ( $Y$ ) of the products for the catalytic hydrogenation of HMF (353 K, 20 bar) over NiAl-R is shown in Figure 3c. The hydrogenation of the aldehyde group generates FDM, which is then further reduced to the fully saturated THFDM derivate via hydrogenation of the furan ring. It was reported that hydrogenation over Ni-Pd/SiO<sub>2</sub><sup>[11]</sup> can also proceed in a reverse order (i.e., initial reduction of the furan ring). However, we did not detect the associated saturated aldehyde by GC-MS, suggesting that this reverse mechanism does not take place under our reaction conditions. In aqueous solution, the hydrogenation of HMF can also produce ring-opening products such as levulinic acid.<sup>[51]</sup> Moreover, cross-polymerisation reactions can lead to the production of soluble polymers and insoluble brown humins.<sup>[52]</sup> But based on analytical results (GC and NMR spectroscopy) no products associated with ring opening or hydrogenolysis (C–O or C–C) were formed under our reaction conditions. Our results are in agreement with the literature, in which catalysts with a high IEP ( $> 7$ )<sup>[5]</sup> and Ni metal<sup>[11]</sup> favour the com-

plete hydrogenation of the furan ring. Moreover, Ni catalysts are commonly used for alkene (e.g., propadiene) or alkyne (e.g., propyne) complete hydrogenation reactions.<sup>[53]</sup> The presence of Ni must favour the adsorption of the intermediate (FDM) with its molecular plane parallel to the surface, which facilitates the hydrogenation of the ring.<sup>[16]</sup>

Figure 4a presents the selectivity ( $S$ ) obtained towards FDM and THFDM as a function of HMF conversion ( $X$ ), combining data obtained over the four catalysts where the mass of catalyst was varied in the range  $0.01 \text{ g} \leq m \leq 0.06 \text{ g}$  and samples were taken every 40 min up to 6 h. The collected data points overlay one another, suggesting that the selectivity is independent of the catalyst's composition, initial mass of catalysts and time but varies consistently with  $X$ . HMF is first converted to FDM, as  $S_{\text{FDM}} = 100\%$  when  $X < 5\%$ . FDM is then progressively converted to THFDM and  $S_{\text{THFDM}} = 40\%$  when  $X \approx 98\%$ . Therefore, the hydrogenation of HMF generates FDM (step 1, Figure 3a) which is then hydrogenated to THFDM (step 2). We also consider in this model the possibility of a direct hydrogenation of HMF to THFDM (step 3):

$$\frac{dY_{\text{HMF}}}{dt} = -(k_1 + k_3) \times Y_{\text{HMF}} \quad (4)$$

$$\frac{dY_{\text{FDM}}}{dt} = k_1 \times Y_{\text{HMF}} - k_2 \times Y_{\text{FDM}} \quad (5)$$

where  $k_i$  is the pseudo-first order rate constant of step  $i$  and  $Y_j$  is the yield of the compound  $j$ . By combination of Equations (4) and (5), Equation (6) is obtained:

$$\frac{dY_{\text{FDM}}}{dY_{\text{HMF}}} = -A + B \times \left( \frac{Y_{\text{FDM}}}{Y_{\text{HMF}}} \right) \text{ with } A = \frac{k_1}{k_1 + k_3} \quad B = \frac{k_2}{k_1 + k_3} \quad (6)$$

which, after integration yields Equation (7):

$$Y_{\text{FDM}} = \frac{A}{1-B} \times (Y_{\text{HMF}}^B - Y_{\text{HMF}}) + C, \quad (7)$$

where  $C$  is a constant. The applicability of this mechanism is assessed in Figure 4b and the model fit to the experimental data ( $R^2 = 0.9989$ ). The values of  $A$  ( $0.912 \pm 0.005$ ) and  $B$  ( $0.138 \pm 0.003$ ) were determined by non-linear mathematical fitting [Eq. (8)]:

$$\frac{k_3}{k_1} = \frac{1-A}{A} \quad \text{and} \quad \frac{k_1}{k_2} = \frac{A}{B} \quad (8)$$

The ratio  $k_3/k_1$  ( $= 0.09$ )  $\ll 1$  indicates a strictly stepwise formation of THFDM whereas  $k_1/k_2$  ( $= 6.60$ )  $\gg 1$  suggests that the hydrogenation of FDM to THFDM is the rate-determining step. This could be caused by a competitive adsorption of FDM with HMF on the catalyst surface; the stronger adsorption of HMF would hinder the reaction of the intermediate FDM. This is consistent with results obtained for the hydrogenation of furfural over Ni catalysts,<sup>[54]</sup> where the authors observed that the rate-determining step was the attack of adsorbed hydrogen on the furan ring of the intermediate (furfuryl alcohol) due to the

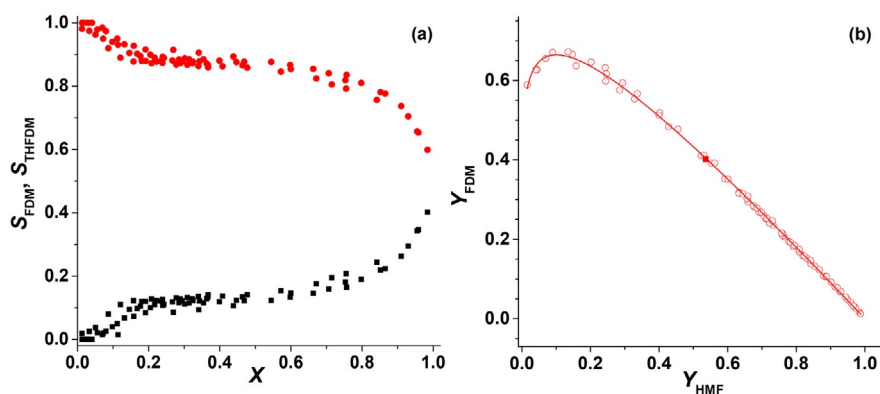


**Figure 4.** (a) Selectivity towards FDM ( $S_{FDM}$ , red) and THFDM ( $S_{THFDM}$ , black) with conversion of HMF (for  $X < 0.99$ ) over the four catalysts. (b) Yield of FDM ( $Y_{FDM}$ ) as a function of yield of HMF ( $Y_{HMF}$ ) and fitting associated with Equation (7) (for  $Y_{HMF} > 0.01$ ).

competitive adsorption of furfural with furfuryl alcohol on the surface.

Figure 4a shows the selectivity associated with the two products up to 98% conversion of HMF; once full conversion is reached, FDM is further converted to THFDM and higher yields of THFDM are achieved. Figure 5 shows the final composition of the solution after 6 h over varying mass ( $m$ ) of NiAl-4R. A rate of THFDM production ( $R_{THFDM}$ ) can be extrapolated from the linear regression of  $Y_{THFDM} = f(m)$  with  $R_{THFDM} = 32 \text{ mmol}_{THFDM} \text{ g}_{Ni}^{-1}$ . High yields of THFDM (>99%) were achieved at longer reaction times (8–12 h) or when increasing the mass of catalyst, as confirmed by GC and NMR spectroscopy (Figure S5). Overall, above 99% yield was achieved in water using our Ni/Al<sub>2</sub>O<sub>3</sub> catalysts (NiAl-R). A result that has not been previously observed in water as studies over Raney nickel are performed in organic solvents.<sup>[12, 13, 19]</sup>

### Stability testing

As most bio-based chemicals can be used in food, cosmetic and pharmaceutical industry, metals have to be completely removed from the solution after reaction; thus, when leaching occurs, expensive separation and purification steps (e.g., ion exchange, filtering) have to be conducted. By preventing pollution at the source, waste formation can be reduced or eliminated and waste treatment circumvented. Therefore, the

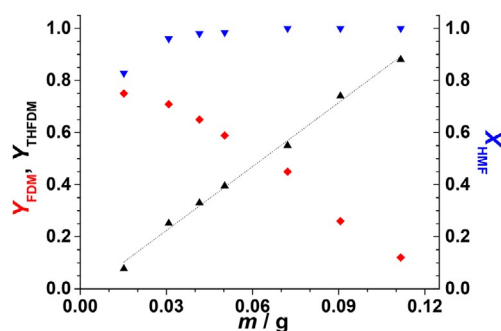


**Figure 5.** Conversion of HMF ( $X$ , blue), yields of FDM ( $Y_{FDM}$ , red) and THFDM ( $Y_{THFDM}$ , black) as a function of the mass of NiAl-4R after 6 h reaction;  $T = 353 \text{ K}$ ,  $P_{H_2} = 20 \text{ bar}$ ,  $C_{i,HMF} \approx 0.04 \text{ mol L}^{-1}$ .

design of a selective process using catalysts resistant to leaching is essential.

The stability of the catalysts was investigated using NiAl-4R as a representative sample. Reaction conditions were chosen to remain below 100% conversion. After reaction, the catalyst was recovered and dried at 393 K under N<sub>2</sub>. Three consecutive runs were conducted, and the composition of the reaction solution after 6 h is presented in Figure 6. The results show that the conversion decreased from circa 80% to 50% after three runs. The process of deactivation can be both of chemical and physical nature, with the main causes including sintering, phase transformation, leaching, coking and poisoning.<sup>[55]</sup> To assess the cause of deactivation, the used catalyst (after run 3) was characterised (Table 5).

The XRD pattern of the catalyst after turnover does not show any additional peaks or changes in peak intensities, indicating no noticeable phase transformation. For supported metals, sintering occurs via migration and coalescence of crystallites with a concomitant increase of the crystallite dimension.<sup>[55]</sup> However, the mean Ni crystallite size did not change before and after turnover ( $d_{Ni} = 10 \text{ nm}$ , Table 5), suggesting that sintering did not occur. The possibility of Ni leaching during the reaction was also assessed; the content of Ni in solution after turnover was measured by ICP and the results obtained were close to the detection limit of 5 ppb, that is, less than 0.002 wt% of Ni leached in the reaction solution. Catalyst

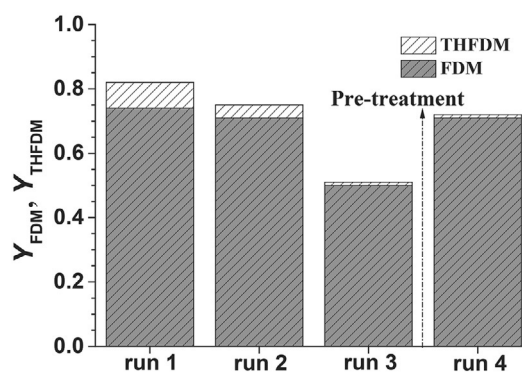


**Figure 6.** Yields of FDM ( $Y_{FDM}$ ) and THFDM ( $Y_{THFDM}$ ) after 6 h reaction over NiAl-4R;  $T = 353 \text{ K}$ ,  $P_{H_2} = 20 \text{ bar}$ ,  $C_{i,HMF} \approx 0.04 \text{ mol L}^{-1}$ ,  $m_{\text{catalyst}} = 0.015 \text{ g}$ .

**Table 5.** Mean Ni crystallite size, amount of Ni leached in solution, carbon and hydrogen content of NiAl-R and mass loss during TGA.

NiAl-4R	$d_{\text{Ni}}^{[a]}$ [nm]	Ni <sup>[b]</sup> leached [wt %]	Content [wt %]		Mass loss <sup>[d]</sup> [wt %]
			C <sup>[c]</sup>	H <sup>[c]</sup>	
before run 1	10(1)	–	0.2	0.6	4
after run 3	10(1)	< 0.002	8.2	2.2	29

[a] Based on Double-Voigt approach, errors report to  $1\sigma$ . [b] Based on ICP analysis of the solution after turnover. [c] Based on CHN analysis. [d] Based on TGA analysis, after heating to 975 K under Ar.

was filtered off from the reaction mixture and the latter was left under  $\text{H}_2$  at 353 K for another 12 h; no further conversion was observed. These results confirm that Ni did not leach into the liquid phase and clearly demonstrate the heterogeneous nature of our catalytic system. It should be mentioned that Nakagawa and Tomishige observed 16% of Ni leached into the liquid phase after conducting the hydrogenation of HMF over Ni–Pd/SiO<sub>2</sub> for 2 h in water.<sup>[11]</sup>

Poisoning usually refers to the obstruction of active sites by molecules/impurities strongly chemisorbed on the surface. The formation of coke results from the condensation, polymerisation and decomposition of molecules on the surface. Elemental analysis (Table 5) showed an increase in carbon (8.0 wt %) and hydrogen (1.6 wt %) content after three runs. The respective TGA curves, measured under Ar, are shown in Figure S6. A total loss of 29 wt % was observed (at 975 K) for the catalyst after three runs, indicating the presence of organic compounds bound to the surface. A loss of activity due to the formation of polymer on the surface was previously reported for the hydrogenation of furanic compounds. Indeed, fast deactivation of Cu-based catalysts was reported for the hydrogenation of furfural due to thermal polymerisation and coking of furfuryl alcohol.<sup>[56]</sup> During the hydrogenation of HMF, it was reported that polymers may form through the loss of formaldehyde from FDM, which was followed by polymerisation.<sup>[15]</sup>

The TGA results suggest that a heat treatment at 773 K should be sufficient to remove the organic impurities. To this end, the catalyst was regenerated by calcination and reduction at 773 K, resulting in significant restoration of catalytic activity. As presented in Figure 6, a conversion of circa 75 % was observed after catalyst regeneration (run 4) which is relatively close to the one obtained after the first run (ca. 80 %). Table 6 summarises the amount of HMF consumed at the end of each run per mass of catalyst ( $R_{\text{HMF}}$ ), where the values obtained follow the trend observed in Figure 6. However, it is interesting

**Table 6.** Ni content of NiAl-4R, HMF consumed per mass of catalyst ( $R_{\text{HMF}}$ ) and mass of Ni ( $R'_{\text{HMF}}$ ) after 6 h reaction.<sup>[a]</sup>

Run	Ni <sup>[b]</sup> [wt %]	$R_{\text{HMF}}$ [mmol <sub>HMF</sub> g <sub>catalyst</sub> <sup>-1</sup> ]	$R'_{\text{HMF}}$ [mmol <sub>HMF</sub> g <sub>Ni</sub> <sup>-1</sup> ]
1	47	98	209
3	33	61	185
4	47	87	184

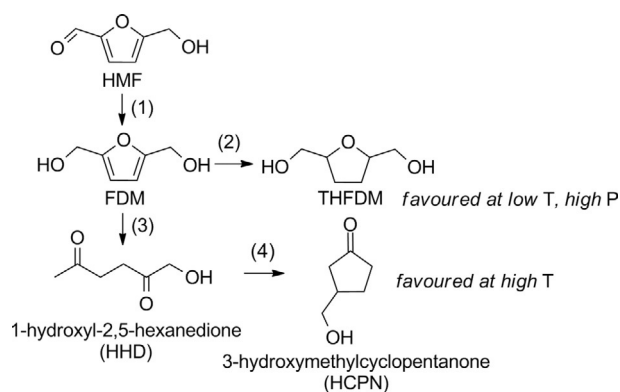
[a] Conditions:  $C_{\text{i,HMF}} \approx 0.04 \text{ mol L}^{-1}$ ;  $m_{\text{catalyst}} = 0.015 \text{ g}$ ;  $T = 353 \text{ K}$ ,  $P_{\text{H}_2} = 20 \text{ bar}$ . [b] Based on ICP analysis after digestion in HCl.

to relate the consumption of HMF to the mass of Ni ( $R'_{\text{HMF}}$ ). Indeed, due to the presence of organic impurities on the surface, the amount of Ni after three runs is lower (Table 6, based on ICP) whereas  $R'_{\text{HMF}}$  is the same for run 3 and run 4. This confirms the removal of the organic impurities from the surface during heat treatment.

### Effect of reaction conditions

The reaction temperature is known to affect catalyst selectivity; when operating at higher temperature (410–450 K) over acid catalysts, cyclopentanone derivatives are predominately formed in aqueous solution (e.g., Au/Nb<sub>2</sub>O<sub>5</sub>)<sup>[57]</sup> whereas the use of an alcohol favours etherification (e.g., Sn-beta zeolite,<sup>[58]</sup> PtSn/Al<sub>2</sub>O<sub>3</sub><sup>[59]</sup>). An increase of temperature from 353 to 413 K was associated with a shift of selectivity towards the ring rearrangement of HMF to a cyclopentanone derivative, 3-hydroxymethylcyclopentanone (HCPN, Scheme 2). This is an important chemical intermediate for the production of pharmaceuticals, insecticides and rubber chemicals.<sup>[57]</sup>

The ring rearrangement of furfural and furfural alcohol to cyclopentanone was studied to a limited extent over supported Pt, Pd, Ru and Ni–Cu catalysts.<sup>[60,61]</sup> These reports suggest that the presence of water, excess of  $\text{H}_2$  and high temperature (e.g., 433 K) are required.<sup>[60,61]</sup> First, furfural is catalytically hydrogenated to furfuryl alcohol. Then, a carbocation is created via the scission of the C–O bond of the furfuryl alcohol. This carbocation is produced under an excess hydrogen and is stabilized by strong interaction with the metal surface. The additional interaction with co-adsorbed water generates cleavage of the C–O bond and rearrangement to cyclopentanone.<sup>[60,61]</sup> There is only one study reporting the conversion of HMF to HCPN<sup>[57]</sup> for which the reactions were conducted over Au, Pt, Pd, Ru supported on Nb<sub>2</sub>O<sub>5</sub>, at 413 K. The authors proposed a similar reaction mechanism, in which the hydrogenation of the aldehyde to the alcohol takes place initially (with formation of FDM), followed by ring opening, which generates 1-hydroxyl-2,5-hexanedione (HHD, Scheme 2); HCPN is then formed by intramolecular aldol condensation of this intermediate. The high yield achieved over Au/Nb<sub>2</sub>O<sub>5</sub> (86 %) was attributed to the presence of Lewis acidic sites that favour ring rearrangement.



**Scheme 2.** Reaction pathway observed for the hydrogenation of HMF ( $C_{\text{i}} \approx 0.04 \text{ mol L}^{-1}$ ) over 0.035 g of NiAl-4R;  $T = 413 \text{ K}$ ,  $P_{\text{H}_2} = 20 \text{ bar}$ .

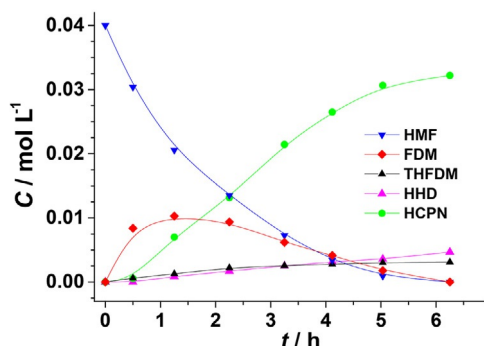


**Figure 7.** Concentrations of HMF, FDM, THFDM, HHD and HCPN as a function of time for the hydrogenation of HMF ( $C_i \approx 0.04 \text{ mol L}^{-1}$ ) over  $0.035 \text{ g}$  of NiAl-4R;  $T = 413 \text{ K}$ ,  $P_{\text{H}_2} = 20 \text{ bar}$ .

Figure 7 presents the dependence of product concentration with time for the hydrogenation of HMF over NiAl-4R at 413 K. The first intermediate, FDM, is formed after hydrogenation of the C=O bond (step 1, Scheme 2). Then, there is a competitive reaction between the full hydrogenation of the ring (with formation of THFDM, step 2, as previously discussed for lower  $T$ ) and ring opening (with formation of HHD, step 3). The following aldol condensation results in the formation of HCPN (step 4). Formation of HCPN and the linear intermediate HHD was verified by GC-MS (Figure S7) and NMR spectroscopy (Figure S8); the results are in complete agreement with the reaction pathway described in literature.<sup>[57,60,61]</sup> The concentration of FDM follows the expected time dependence for reaction intermediates: first it increases with time (1–2 h) but then decreases as it is consumed and converted to products (THFDM and HCPN). The reaction conditions used (i.e., water, excess of  $\text{H}_2$ , high temperature) favour the aldol condensation and formation of HCPN, which is in agreement with literature.<sup>[60,61]</sup> We thus report for the first time the synthesis of HCPN over Ni catalysts as opposed to the use of noble metal catalysts.<sup>[57]</sup> In addition this is the first study conducted over a base metal catalyst where yields up to 80% were achieved after 6 h reaction (Figure 7).

Table 7 summarises the effect of temperature and pressure on the catalytic results. Entry A corresponds to the result presented above at 353 K where a mixture of FDM and THFDM is obtained. Increasing the temperature (entry B, 393 K) results in two competitive reactions: hydrogenation of the ring (step 2) and ring opening (step 3, followed by step 4), with the former becoming predominant at 413 K (entry C). When operating at

**Table 7.** Effect of temperature, pressure and mass of catalyst on conversion ( $X$ ) and yields of products for the hydrogenation of HMF over NiAl-4R; results after 6 h reaction.

Reaction	$T$ [K]	$P_{\text{H}_2}$ [bar]	$m_{\text{catalyst}}$ [mg]	$X$ [%]	Yield [%]			
					FDM	THFDM	HHD	HCPN
A	353	20	31	96	25	71	0	0
B	393	20	35	100	5	26	5	64
C	413	20	35	100	0	8	11	81
D	413	20	10	53	11	3	2	37
E	413	3	30	49	21	3	3	22
F	413	56	30	100	0	16	15	69

413 K, a decrease of initial mass of catalyst (entry D) is associated with a decrease in conversion, with HCPN still being the major product. The partial pressure of  $\text{H}_2$  ( $P_{\text{H}_2}$ ) was varied to assess a possible effect on selectivity. At lower pressure ( $P_{\text{H}_2} = 3 \text{ bar}$ , entry E), the conversion is lower and higher concentration of intermediates (FDM) is observed. On the contrary, higher pressure ( $P_{\text{H}_2} = 56 \text{ bar}$ , entry F) favours the formation of THFDM (step 2) over HCPN. When running the reaction at even higher temperatures ( $> 433 \text{ K}$ ), cross-polymerisations take place leading to the production of insoluble brown humins. Therefore, the selectivity depends mainly on temperature and conversion and to some extent on  $\text{H}_2$  partial pressure; we observed that the hydrogenation of HMF towards THFDM is favoured with an increase in pressure and a decrease in temperature.

## Conclusions

We reported the synthesis of Ni-on- $\text{Al}_2\text{O}_3$  catalysts derived from Ni-Al layered double hydroxides and their use for the promotion of the selective liquid-phase hydrogenation of 5-hydroxymethylfurfural to tetrahydrofuran-2,5-diylidimethanol in water. The layered double hydroxides were successfully synthesised by precipitation using urea and full precipitation occurred. The XRD patterns were fitted using the  $R\bar{3}m$  space group (rhombohedral symmetry), revealing that the lattice parameter  $a$  decreased with increasing Al content following Vegard's law. Calcination of the precursors caused the removal of interlayer hydroxyl and carbonate groups and formation of NiO particles. The following reduction of  $\text{Ni}^{2+}$  to  $\text{Ni}^0$  occurred during pre-treatment with  $\text{H}_2$  at 773 K and was hindered by the presence of  $\text{Al}^{3+}$  incorporated into the NiO lattice. The four reduced mixed-oxide catalysts exhibited high Ni contents (up to 68%) and had a lamellar structure with well-dispersed Ni metal nanoparticles ( $d_{\text{Ni}} = 10\text{--}14 \text{ nm}$ ) on an Al-rich amorphous component. We demonstrated the applicability of pseudo-first-order reaction kinetics for HMF conversion to THFDM and observed that the respective rate constants per mass of Ni are equivalent for the four catalysts. Stability tests showed that Ni did not leach into the liquid phase and that sintering did not take place after three consecutive runs. The decrease in conversion was associated with the formation of coke resulting from polymerisation; the removal of the coke by heat treatment regenerated the activity. We also established that selectivity depended mainly on temperature and conversion and to some extent on  $\text{H}_2$  pressure. We achieved 100% yield of the target THFDM when working at 353 K in water; the use of higher temperature generated the formation of 3-hydroxymethylcyclopentanone, an important intermediate chemical.

## Experimental Section

### Catalyst preparation

Four catalyst precursors  $\text{Ni}_{(1-x)}\text{Al}_x(\text{OH})_2(\text{CO}_3)_{x/2} \cdot m\text{H}_2\text{O}$ , with  $0.24 \leq x \leq 0.47$  and  $0.3 \leq m \leq 0.7$ , were prepared by co-precipitation using

urea based on the method developed by Costantino et al.<sup>[29]</sup> A known mass of powdered urea (Sigma) was placed in a reaction flask (250 mL) with distilled water (50 mL). A mixture of 1.5 M aqueous solutions of  $\text{AlCl}_3 \cdot 6\text{H}_2\text{O}$  (Fluka,  $\geq 99.0$  wt% purity) and  $\text{NiCl}_2 \cdot 6\text{H}_2\text{O}$  (Aldrich, 99.9 wt% purity) were added. The volumes of the solutions and the mass of urea were appropriately chosen to have the Al ratios ( $x = n_{\text{Al}}/(n_{\text{Ni}} + n_{\text{Al}})$ ) in the range 0.24–0.47 and  $n_{\text{urea}}/(n_{\text{Ni}} + n_{\text{Al}}) = 3.3$ . The flasks were placed in a Radley Carousel 6 Plus station, stirred at 750 rpm and heated to 368 K at 1  $\text{Kmin}^{-1}$  under reflux. After aging for 65 h, the solutions were cooled to ambient temperature and filtered. The precipitated materials were left in suspension with  $\text{NH}_4\text{HCO}_3$  for 5 h (to remove any residual Cl), then filtered, washed and dried for 3 h at 353 K (heating rate 2  $\text{Kmin}^{-1}$ ). The solids were then ground and dried for 5 h at 393 K (heating rate 2  $\text{Kmin}^{-1}$ ); the precursors are denominated NiAl-ZP with  $Z = 1, 2, 3$  and 4; The number  $Z$  relates to the Al content ( $x$ ) where NiAl-1P corresponds to the precursor with the lowest Al content. The samples were placed in a furnace (0.35 g of powder per crucible) and successively calcined (under air, 75  $\text{mLmin}^{-1}$ , NiAl-C) and reduced (under pure  $\text{H}_2$ , 100  $\text{mLmin}^{-1}$ ) for 5 h at 773 K (heating rate 5  $\text{Kmin}^{-1}$ ); the catalysts were then passivated ( $< 1\%$  v/v  $\text{O}_2/\text{N}_2$ , 100  $\text{mLmin}^{-1}$ ) at room temperature for 3 h (NiAl-ZR).

### Catalyst characterization

Total surface area (SA), pore volume (PV) and pore size distribution of the precursors and catalysts were determined by volumetric  $\text{N}_2$  adsorption at 77 K using a Tristar II micromeritics. Thermal gravimetric analysis (TGA) was performed using a Q500 TA Instruments; ca. 10 mg of samples was heated to 1023 K at 5  $\text{Kmin}^{-1}$  under 50 mL of air or Ar and changes in mass were recorded. Temperature-programmed reduction (TPR) was measured using the commercial CHEM-BET 3000 (Quantachrome) unit; 50 mg of samples were loaded into a Quartz cell, heated in 30  $\text{mLmin}^{-1}$  5% v/v  $\text{H}_2/\text{N}_2$  at 5  $\text{Kmin}^{-1}$  to 773–1073 K and changes in  $\text{H}_2$  consumption were monitored by means of a thermal conductivity detector (TCD). C and H contents of the materials were determined by microanalytical procedures using a Thermo EA1112 Flash CHNS Analyser. Al and Ni contents of the catalysts and solutions were measured by inductively coupled plasma-optical emission spectrometry (ICP-OES) after digesting 25 mg of the material in 10 mL of HCl (37%) for 4 h and diluting it with water (1:10 v/v).

The precursors and catalysts were sputter coated using Au and images were recorded by using a Hitachi S-4800 Field-Emission Scanning Electron Microscope; Ni, Al and Cl content were obtained by SEM-EDX. A small amount of sample was deposited on the C film of a Cu grid and Ni particle size distribution was obtained using a JEOL 2100 transmission electron microscope (TEM).

The precursors were ground and combined using oven-dried KBr and pressed into a disc. The spectra of the samples were recorded by accumulating 64 scans at 4  $\text{cm}^{-1}$  resolution between 400 and 4000  $\text{cm}^{-1}$  using a Fourier Transform Infrared (FTIR) Bruker Tensor 27.

Powder X-ray diffractograms (XRD) data were collected in reflection geometry on a Panalytical X'Pert Pro diffractometer with  $\text{CoK}_{\alpha 1}$  radiation ( $\lambda = 1.7890 \text{ \AA}$ ). Samples were scanned at  $0.023^\circ \text{ s}^{-1}$  over the range  $10^\circ \leq 2\theta \leq 80^\circ$  for phase identification using the reference standards, that is, Ni (Card No. 73–1519) and NiO (70–0989). Samples were mixed with  $\text{LaB}_6$  as an internal standard and the powders were scanned over the range  $10^\circ \leq 2\theta \leq 120^\circ$  for complete pattern fitting; the lattice parameters of the materials were obtained by performing Pawley refinement using Topas academic software, with the cell parameter of  $\text{LaB}_6$  (space group  $Pm\bar{3}m$ ;  $a =$

4.15700  $\text{Å}$ ) fixed. The mean crystallite sizes ( $d_{\text{Ni}}$ ) were determined using the Double-Voigt approach based on the method of Balzar et al.<sup>[62,63]</sup> and assuming a mono-disperse system of spheres. Specific Ni surface areas were obtained using Equation (9)

$$SA_{\text{Ni}} = \frac{6}{\rho \times d_{\text{Ni}}}, \quad (9)$$

with  $\rho$  being the Ni-specific mass.

The IEPs were determined by measuring the change in zeta potential as a function of pH value. In each case, circa 10 mg of catalyst was dispersed in 10 mL of distilled water; the zeta potentials were obtained by measuring the electrophoretic mobility of the particle using a Malvern Zetasizer Nano ZSP Instrument. The pH value was controlled using a MPT-2 titrator (adding HCl or NaOH, 0.025 M), and ten measurements were conducted between pH 6 and 12.

### Catalytic testing

Reactions were carried out in a batch stirred stainless steel Parr 5000 reactor. In a typical experiment, 0.01–0.14 g catalyst and 45 mL aqueous solution of reactant ( $C = 0.02\text{--}0.04 \text{ molL}^{-1}$ ) were charged in a glass liner. The reactor was then closed, flushed under  $\text{N}_2$ , stirred (600 rpm) and heated to reaction temperature (353–413 K). After stabilisation of the temperature (ca. 1 h),  $\text{H}_2$  was added and the reactor was kept under constant pressure (5–60 bar). The product composition and identification was determined using an Agilent Technologies 7890 A gas chromatograph equipped with a flame ionisation detector (FID) and an Agilent 6890N GC equipped with a 5973 MSD, respectively. A DB-WAXetr 60  $\text{m} \times 0.25 \text{ mm i.d.}$ , 0.25  $\mu\text{m}$  film thickness capillary column (Agilent J&W) was employed in both cases. Repeated reactions with different samples from the same batch of catalyst delivered a product composition that was reproducible to within  $\pm 5\%$ . A blank test conducted without catalyst did not result in any detectable conversion. HMF (Sigma,  $\geq 99$  wt% purity) was used as received without further purification. FDM (Manchester organics) and THFDM (Ambinter) were used for identification and calibration of products.

HMF conversion ( $X$ ) at time  $t$  was calculated using Equation (10):

$$X = \frac{C_{\text{HMF, in}} - C_{\text{HMF}}}{C_{\text{HMF, in}}} \quad (10)$$

$C_{\text{HMF, in}}$  and  $C_{\text{HMF}}$  are the initial concentration and the concentration at time  $t$  of HMF in solution, respectively. The selectivity ( $S$ ) and yield ( $Y$ ) with respect to FDM as an example, are given by Equation (11):

$$S_{\text{FDM}} = \frac{C_{\text{FDM}}}{C_{\text{HMF, in}} - C_{\text{HMF}}} \quad \text{and} \quad Y_{\text{FDM}} = S_{\text{FDM}} \times X \quad (11)$$

Identification of THFDM and 3-hydroxymethyl cyclopentanone was performed by  $^1\text{H}$  and  $^{13}\text{C}$  NMR spectroscopy using a Bruker Avance III HD NMR spectrometers operating at 400 MHz proton frequency. Water was removed from the solutions using a rotary evaporator, and the compounds left were diluted in DMSO; chemicals shifts are reported relative to residual solvent.

### Acknowledgements

This work was supported by the Engineering and Physical Sciences Research Council (EPSRC), UK (EP/K014749).

**Keywords:** 5-hydroxymethylfurfural · hydrogenation · layered compounds · nickel · water

- [1] E. de Jong, R. J. A. Gosselink, *Lignocellulose-Based Chemical Products in Bioenergy Research: Advances and Applications* (Eds.: V. K. Gupta, C. P. Kubicek, J. Saddler, F. Ku, M. G. Tuohy), Elsevier, Amsterdam, **2014**, pp. 277–313.
- [2] R.-J. van Putten, J. C. van der Waal, E. de Jong, C. B. Rasrendra, H. J. Heeres, J. G. de Vries, *Chem. Rev.* **2013**, *113*, 1499–1597.
- [3] A. A. Rosatella, S. P. Simeonov, R. F. M. Frade, C. A. M. Afonso, *Green Chem.* **2011**, *13*, 754–793.
- [4] A. Corma, S. Iborra, A. Velty, *Chem. Rev.* **2007**, *107*, 2411–2502.
- [5] M. Besson, P. Gallezot, C. Pinel, *Chem. Rev.* **2014**, *114*, 1827–1870.
- [6] C. Moreau, M. N. Belgacem, A. Gandini, *Top. Catal.* **2004**, *27*, 11–30.
- [7] J. N. Chheda, G. W. Huber, J. A. Dumesic, *Angew. Chem. Int. Ed.* **2007**, *46*, 7164–7183; *Angew. Chem.* **2007**, *119*, 7298–7318.
- [8] L. Hu, G. Zhao, W. Hao, X. Tang, Y. Sun, L. Lin, S. Liu, *RSC Adv.* **2012**, *2*, 11184–11206.
- [9] T. Buntara, S. Noel, P. H. Phua, I. Melián-Cabrera, J. G. de Vries, H. J. Heeres, *Top. Catal.* **2012**, *55*, 612–619.
- [10] V. Schiavo, G. Descotes, J. Mentech, *Bull. Soc. Chim. Fr.* **1991**, 704–711.
- [11] Y. Nakagawa, K. Tomishige, *Catal. Commun.* **2010**, *12*, 154–156.
- [12] J. G. D. Vries, Teddy, P. Huat Phua, I. V. Melián-Cabrera, H. J. Heeres, Preparation of caprolactone caprolactam, 2,5-tetrahydrofuran-dimethanol, 1,6-hexanediol or 1,2,6-hexanetriol from 5-hydroxymethyl-2-furfuraldehyde, Netherlands Organisation For Scientific Research, **2011**, Patent WO 2011149339 A1.
- [13] T. J. Connolly, J. L. Considine, Z. Ding, B. Forsatz, M. N. Jennings, M. F. MacEwan, K. M. McCoy, D. W. Place, A. Sharma, K. Sutherland, *Org. Process Res. Dev.* **2010**, *14*, 459–465.
- [14] X. Hu, R. J. M. Westerhof, L. P. Wu, D. H. Dong, C. Z. Li, *Green Chem.* **2015**, *17*, 219–224.
- [15] R. Alamillo, M. Tucker, M. Chia, Y. Pagán-Torres, J. Dumesic, *Green Chem.* **2012**, *14*, 1413–1419.
- [16] S. Yao, X. Wang, Y. Jiang, F. Wu, X. Chen, X. Mu, *ACS Sustainable Chem. Eng.* **2014**, *2*, 173–180.
- [17] J. Jae, W. Q. Zheng, R. F. Lobo, D. G. Vlachos, *ChemSusChem* **2013**, *6*, 1158–1162.
- [18] Y. Román-Leshkov, C. J. Barrett, Z. Y. Liu, J. A. Dumesic, *Nature* **2007**, *447*, 982–U985.
- [19] T. Buntara, S. Noel, P. H. Phua, I. Melián-Cabrera, J. G. de Vries, H. J. Heeres, *Angew. Chem. Int. Ed.* **2011**, *50*, 7083–7087; *Angew. Chem.* **2011**, *123*, 7221–7225.
- [20] T. Buntara, I. Melián-Cabrera, Q. Tan, J. L. G. Fierro, M. Neurock, J. G. de Vries, H. J. Heeres, *Catal. Today* **2013**, *210*, 106–116.
- [21] H. Xiong, H. N. Pham, A. K. Datye, *Green Chem.* **2014**, *16*, 4627–4643.
- [22] A. E. Marteel-Parish, M. A. Abraham, *Green Chemistry and Engineering: A Pathway to Sustainability*, Wiley, American Institute of Chemical Engineers, Inc., New Jersey, **2013**.
- [23] F. M. Kerton, R. Marriott, *Alternative Solvents for Green Chemistry*, RSC Publishing, Cambridge, **2013**, pp. 001–226.
- [24] A. Monzón, E. Romeo, A. J. Marchi, *Hydrogenation catalysis by mixed oxides prepared from LDHs, in Layered double hydroxides, present and future* (Ed.: V. Rives), Nova Science Publishers, Inc., New York, **2001**, pp. 367–434.
- [25] F. Basile, P. Benito, G. Fornasari, A. Vaccari, *Appl. Clay Sci.* **2010**, *48*, 250–259.
- [26] F. Kovanda, T. Rojka, P. Bezdička, K. Jiráťová, L. Obalová, K. Pacultová, Z. Bastl, T. Grygar, *J. Solid State Chem.* **2009**, *182*, 27–36.
- [27] C. Rudolf, B. Dragoi, A. Ungureanu, A. Chiriac, S. Royer, A. Nastru, E. Dumitriu, *Catal. Sci. Technol.* **2014**, *4*, 179–189.
- [28] F. Cavani, F. Trifirò, A. Vaccari, *Catal. Today* **1991**, *11*, 173–301.
- [29] U. Costantino, F. Marmottini, M. Nocchetti, R. Vivani, *Eur. J. Inorg. Chem.* **1998**, 1439–1446.
- [30] M. Khoudiakov, M. C. Gupta, S. Deevi, *Appl. Catal. A* **2005**, *291*, 151–161.
- [31] M. R. Othman, Z. Helwani, Martunus, W. J. N. Fernando, *Appl. Organomet. Chem.* **2009**, *23*, 335–346.
- [32] P. Basu, M. Johnson, *The integrated approach to chemistry laboratory*, DEStech Publications, Inc., **2009**, pp. 21.
- [33] S. Kannan, A. Narayanan, C. S. Swamy, *J. Mater. Sci.* **1996**, *31*, 2353–2360.
- [34] S. K. Sharma, P. K. Kushwaha, V. K. Srivastava, S. D. Bhatt, R. V. Jasra, *Ind. Eng. Chem. Res.* **2007**, *46*, 4856–4865.
- [35] J. T. Klopogge, R. L. Frost, *J. Solid State Chem.* **1999**, *146*, 506–515.
- [36] S. Miyata, *Clay. Clay Miner.* **1980**, *28*, 50–56.
- [37] G. W. Brindley, C.-C. Kao, *Phys. Chem. Miner.* **1984**, *10*, 187–191.
- [38] F. Medina, R. Dutartre, D. Tichit, B. Coq, N. T. Dung, P. Salagre, J. E. Sueiras, *J. Mol. Catal. A* **1997**, *119*, 201–212.
- [39] F. Malherbe, L. Bigey, C. Forano, A. de Roy, J.-P. Besse, *J. Chem. Soc. Dalton Trans.* **1999**, 3831–3839.
- [40] A. C. C. Rodrigues, C. A. Henriques, J. L. F. Monteiro, *Mater. Res.* **2003**, *6*, 563–568.
- [41] Y. H. Lin, M. O. Adebajo, R. L. Frost, J. T. Klopogge, *J. Therm. Anal. Calorim.* **2005**, *81*, 83–89.
- [42] F. Trifirò, A. Vaccari, O. Clause, *Catal. Today* **1994**, *21*, 185–195.
- [43] A. Atkinson, C. Monty, *Grain boundary diffusion in ceramics in Surfaces and interfaces of ceramic materials* (Eds.: L.-C. Dufour, C. Monty, G. Petot-Ervas), Kluwer Academic Publishers, Dordrecht, **1989**, pp. 280.
- [44] Q. H. Liu, B. C. Wang, C. X. Wang, Z. J. Tian, W. Qu, H. J. Ma, R. S. Xu, *Green Chem.* **2014**, *16*, 2604–2613.
- [45] S. Miyata, *Clay. Clay Miner.* **1983**, *31*, 305–311.
- [46] M. D. Argyle, C. H. Bartholomew, *Catalysts* **2015**, *5*, 145–269.
- [47] M. Kosmulski, *Adv. Colloid Interface Sci.* **2009**, *152*, 14–25.
- [48] U. K. Singh, M. A. Vannice, *Appl. Catal. A* **2001**, *213*, 1–24.
- [49] K. Lourvanij, PhD thesis, Partial dehydration of glucose to oxygenated hydrocarbons in molecular-sieving catalysts, Oregon State University, **1995**.
- [50] J. Tuteja, H. Choudhary, S. Nishimura, K. Ebitani, *ChemSusChem* **2014**, *7*, 96–100.
- [51] X. L. Tong, Y. Ma, Y. D. Li, *Appl. Catal. A* **2010**, *385*, 1–13.
- [52] J. Lewkowski, *Arhivoc* **2001**, 17–54.
- [53] S. Abelló, D. Verboekend, B. Bridier, J. Pérez-Ramírez, *J. Catal.* **2008**, *259*, 85–95.
- [54] Y. Nakagawa, H. Nakazawa, H. Watanabe, K. Tomishige, *ChemCatChem* **2012**, *4*, 1791–1797.
- [55] P. Forzatti, L. Lietti, *Catal. Today* **1999**, *52*, 165–181.
- [56] J.-P. Lange, E. van der Heide, J. van Buijtenen, R. Price, *ChemSusChem* **2012**, *5*, 150–166.
- [57] J. Ohyama, R. Kanao, A. Esaki, A. Satsuma, *Chem. Commun.* **2014**, *50*, 5633–5636.
- [58] J. Jae, E. Mahmoud, R. F. Lobo, D. G. Vlachos, *ChemCatChem* **2014**, *6*, 508–513.
- [59] M. Balakrishnan, E. R. Sacia, A. T. Bell, *Green Chem.* **2012**, *14*, 1626–1634.
- [60] M. Hronec, K. Fulajtarová, T. Liptaj, *Appl. Catal. A* **2012**, *437*, 104–111.
- [61] Y. L. Yang, Z. T. Du, Y. Z. Huang, F. Lu, F. Wang, J. Gao, J. Xu, *Green Chem.* **2013**, *15*, 1932–1940.
- [62] D. Balzar, N. Audebrand, M. R. Daymond, A. Fitch, A. Hewat, J. I. Langford, A. Le Bail, D. Louer, O. Masson, C. N. McCowan, N. C. Popa, P. W. Stephens, B. H. Toby, *J. Appl. Crystallogr.* **2004**, *37*, 911–924.
- [63] D. Balzar, H. Ledbetter, *J. Appl. Crystallogr.* **1993**, *26*, 97–103.

Received: September 9, 2015

Revised: December 1, 2015

Published online on February 12, 2016